EUROFUSION WPMST1-CP(16) 15038

J-M Noterdaeme et al.

Ion Cyclotron Range of Frequency Power Challenges and Solutions

Preprint of Paper to be submitted for publication in
Proceedings of 26th IAEA Fusion Energy Conference

This work has been carried out within the framework of the EUROfusion Consortium and has received funding from the Euratom research and training programme 2014-2018 under grant agreement No 633053. The views and opinions expressed herein do not necessarily reflect those of the European Commission.

This document is intended for publication in the open literature. It is made available on the clear understanding that it may not be further circulated and extracts or references may not be published prior to publication of the original when applicable, or without the consent of the Publications Officer, EUROfusion Programme Management Unit, Culham Science Centre, Abingdon, Oxon, OX14 3DB, UK or e-mail Publications.Officer@euro-fusion.org

Enquiries about Copyright and reproduction should be addressed to the Publications Officer, EUROfusion Programme Management Unit, Culham Science Centre, Abingdon, Oxon, OX14 3DB, UK or e-mail Publications.Officer@euro-fusion.org

The contents of this preprint and all other EUROfusion Preprints, Reports and Conference Papers are available to view online free at http://www.euro-fusionscipub.org. This site has full search facilities and e-mail alert options. In the JET specific papers the diagrams contained within the PDFs on this site are hyperlinked

Ion Cyclotron Range of Frequency Power Challenges and Solutions

J.-M. Noterdaeme[1,2], V. Bobkov[1], H. Fuenfgelder[1], R. D'Inca[1], R. Ochoukov[1], J. Jacquot[1], W. Tierens[1], W. Zhang[1,2,5], H. Faugel[1], T. Vierle[1]. I. Zammuto[1], K. Crombé[2,3], I. Stepanov[3] R. Ragona[2,3], A. Messiaen[3], D. Van Eester[3], A. A. Tuccillo[4], O. Tudisco[4], G. Rocchi[4], A. Mancini[4], O. D'Arcangelo[4], Q. Yang[5], Y. Wang[5], Y. Chen[5], D. Milanesio[6], R. Maggiora[6], L. Colas[7], S. Heuraux[8], E. Faudot[8], J. Moritz[8], A. Silva[9], D. Aguiam[9], the ASDEX Upgrade[1] and EUROfusion MST1* Teams

[1] Max-Planck-Institut für Plasmaphysik, Boltzmannstr. 2, D-85748 Garching, Germany
[2] Ghent University, Applied Physics Department, B-9000 Gent, Belgium
[3] LPP-ERM/KMS, B-1000 Brussels, Belgium
[4] ENEA, Frascati, Italy
[5] ASIPP, Institute of Plasma Physics, Chinese Academy of Sciences, Hefei, China
[6] Politecnico de Torino, Torino, Italy
[7] CEA, IRFM, F-13108 Saint-Paul-Lez-Durance, France
[8] IJL UMR 7198 CNRS-Université de Lorraine, BP70239, F-54506 Vandoeuvre, France
[9] Instituto de Plasmas e Fusão Nuclear, IST, 1049-001 Lisboa, Portugal,
* See the author list of "Overview of progress in European Medium Sized Tokamaks towards an integrated plasma-edge/wall solution" by H. Meyer et al., to be published in Nuclear Fusion Special issue: overview and summary reports from the 26th Fusion Energy Conference (Kyoto, Japan, 17-22 October 2016)

E-mail contact of main author: noterdaeme@ipp.mpg.de

Abstract. The use of power in the Ion Cyclotron Range of Frequency (ICRF) to heat the plasma has encountered challenges: the *sensitivity to the plasma edge density profile,* with the difficulty to couple power to the plasma and the *enhanced plasma-antenna interaction* with, among others, the resulting impurity production. These challenges have essentially been solved.

Problems related to the *sensitivity to the plasma edge density profiles*, were encountered when strong ELMs changed massively the antenna coupling and affected the operation of the generators, and when low edge density lead to insufficient coupling and high voltages. The first problem has long been solved with the use of 3-dB couplers. The second problem was addressed in recent experiments, where local gas puffing helped to tailor the density profile and increase the coupling. A systematic study confirmed that the coupling can be calculated if the local density profile is known. The development of a theoretical approach to model the local density profile that was benchmarked against the recently acquired ability to measure locally the density profile is developing into a predictive capability to calculate and optimize the coupling also for future machines.

The hypothesis concerning the *enhanced plasma-antenna interactions* is that they are mainly due to RF sheaths at the antenna and that those sheaths are a consequence of induced current driven at inappropriate locations. New 3-strap antennas in ASDEX Upgrade were designed to reduce those unwanted currents. This approach leads indeed to a strong reduction of the impurity production. Whereas, with the original W-coated 2-strap antennas, the increase with ICRF of the W impurity concentration in the edge plasma was about twice the increase as when the B-coated 2-strap antennas were in operation, with the new 3-strap antennas (still W-coated) the W concentration is not higher than when using the B-coated 2-strap antennas. Direct measurements of the impurity production at the limiters of the W-coated antennas show a reduction by a factor of 2 between the 3-strap and the 2-strap antennas. Theoretical approaches to model in detail the formation of the sheaths are being developed and are being checked against measurements on ASDEX Upgrade. IShTAR, a dedicated test stand to measure the electric fields will further allow to benchmark the codes.

These newly developed and benchmarked code capabilities will benefit the design of antennas for future machines.

1. Introduction

The two main challenges to the use of ICRF power, in particular in all-metal machines, have been successfully addressed: the *sensitivity of the coupling to the plasma edge density profile* with the corresponding difficulty to couple power to the plasma and the *enhanced plasma-antenna interaction* with, among others, an increased impurity production.

2. Sensitivity to the plasma edge profile

Because the plasma wave (the fast wave) used to couple power from the antenna to the plasma centre is evanescent below a minimum plasma density, this wave may, depending on the density profile in front of the antenna, only start to propagate at a distance from the antenna. This makes the electrical impedance of the antenna sensitive to the density profile.

2.1. Strong coupling variations with ELMs

The first consequence is that, when the changes in the edge density profile are large, for example due to ELMs, the electrical parameters of the antenna can vary by up to an order of magnitude. The matching system, meant to avoid power reflection to the generator, can often be too slow to adapt to these large variations. The safety systems then turn off generators. The use of 3dB couplers [1, 2, 3], which direct the reflected power to a dummy load or the use of

conjugate-T matching [4], which reduce the variation of the antenna parameters due to the density changes, solves this problem. Furthermore, for larger machines and new antenna concepts [5] ICRF systems can be designed where the change of the density profile has a negligible effect on the antenna parameters.

2.2. Reduced coupling at low edge density

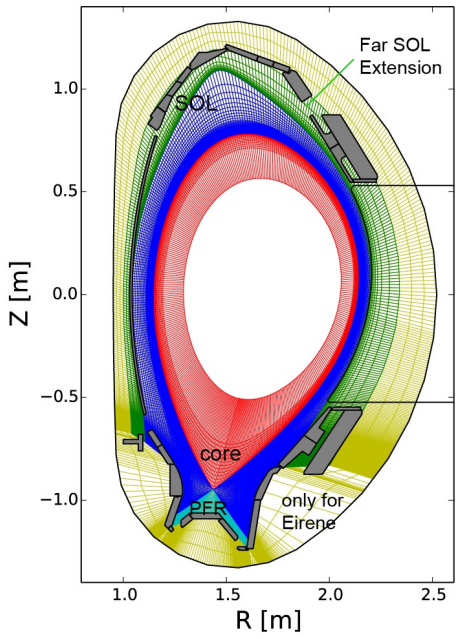

FIG. 1. Poloidal cross-section of the EMC3-EIRENE computational grid for AUG, reproduced from [10].

The second consequence of the wave starting to propagate at some distance from the antenna is that the reduced coupling can result in large electric fields and high voltages to launch a given amount of power in the plasma. In recent experiments, local gas puffing was used to tailor the density profile and increase the coupling. We have developed the means to reliably calculate the resulting coupling and the gas puffing needed. A systematic study [6] confirmed that the coupling can be calculated if the *local* density profile is known. The study compared the complex voltage reflection coefficient Γ on each antenna port, measured with voltage/current probes (~3 m from each input port) and directional couplers (on the matched line) on antennas #1, #2 and #3 of AUG and computed using the ICRF antenna code TOPICA (TOrino Politecnico Ion Cyclotron Antenna) [7]. The radial electron density profile, obtained from the DCN interferometer (for the core) and lithium beam emission spectroscopy (for the SOL) measurements, was used as input along with a realistic 3 dimensional (3D) antenna model. The density profile was ELM-synchronized to remove the fast fluctuations in coupling during ELMs. Seven AUG discharges were used with different plasma parameters and antenna frequencies. The code reproduced the correct trend in coupling in a significant majority of cases. The best agreement in $|\Gamma|$ was found on antenna #3 (calculated value within 3% of measured value, averaged over a shot) while for antennas #1 and #2 the results were within 10%. Since both DCN and Li-beam diagnostics are close to antenna #3 (sector 10), while antennas #1 and #2 are on the opposite side of the torus (sectors 2 and 4), the density profile was reconstructed from measurements taken close to antenna #3. This suggested that the density profile in front of the antennas may depend on the toroidal location and that the local profile needs to be known in order to accurately predict the antenna coupling. Local gas puffing was also shown to affect an antenna in the vicinity, more than would be expected from the density change measured further away. We thus developed a theoretical approach to calculate the local density profile, including local gas puffing.

The three-dimensional (3D) edge plasma code EMC3-EIRENE has been used to simulate the spatial inhomogenous electron density. The code couples self-consistently the Edge Monte Carlo 3D plasma fluid code (EMC3) [8] and the kinetic neutral Monte Carlo code (EIRENE) [9]. EMC3 solves a set of time-independent Braginskii's equations for mass, parallel momentum, electron and ion energy, and EIRENE computes the Boltzmann equation. The simulation model includes a toroidal 360° computational grid, the essential plasma facing

components, the gas sources and sinks. The EMC3 grid is composed of the core, Scrape-Off Layer (SOL) and Private Flux Region (PFR), while the EIRENE grid is further extended to fill the whole vessel. An example of the poloidal cross-section of the EMC3-EIRENE computational grids for AUG is shown in *FIG. 1*. In a first step, the edge plasma parameters during divertor gas puffing in the code are matched to the measurements of the upstream profiles (the mid-plane density and temperature) and downstream profiles (the particle and power fluxes to the divertor). The gas source is then switched to other locations (typically top

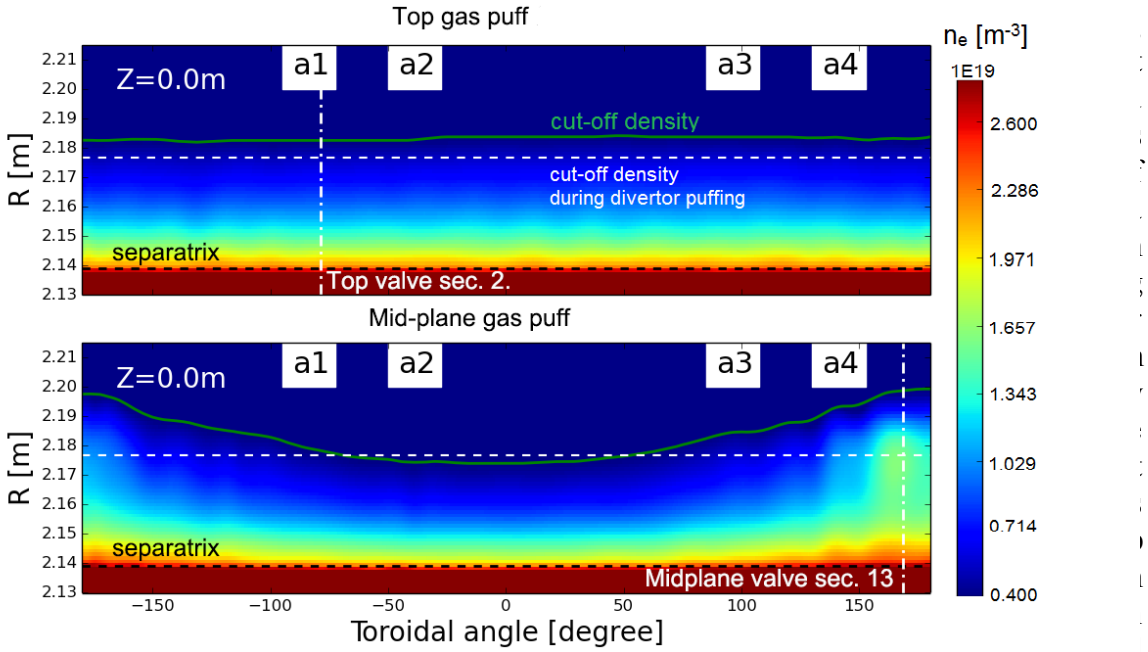

FIG. 3 Toroidal cross-sections of the edge density during top and mid-plane gas puffing in AUG H-mode plasmas. The white dashed line is the cut-off density during divertor gas puffing and is used as a reference, and the green line is the cut-off density during top or mid-plane gas puffing. The vertical dash-dotted lines represent the toroidal positions of the gas valves. Reproduced from

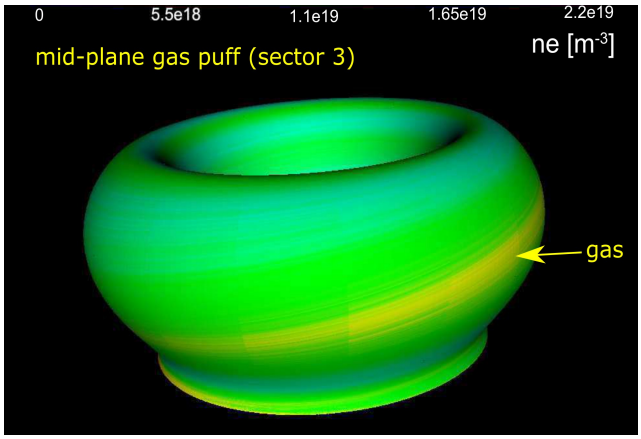

FIG. 2. 3D view of the SOL density at $\rho_{pol} = 1.08$ during mid-plane gas puffing.

This diagnostic has been installed on ASDEX Upgrade in the new 3-strap ICRF antenna (#4, sector 12) and is able to provide local measurements of electron density profiles right in front of the antenna. Three of ten available microwave antenna pairs are fully instrumented. They are located near the bottom, middle and top regions of the ICRF antenna radiating surface and allow the study the local effects of the gas puffing, including the poloidal variations. Density profiles can be measured from zero density up to 2×10^{19} m^{-3}, depending on the local magnetic field, at a maximum repetition rate of 25 µs between profiles [12].

An example of the comparison is shown in *FIG. 4,* where edge density profiles at z = 0 m are compared with reflectometer measu-rements during different gas puffing scenarios in AUG L-mode plasmas (the discharge is without ICRF, so it does not need to take into account the effect of the ICRF on the density, for a self-consistent approach, see section 3.2). The mid-plane gas valve in sector 13 (MID13) is located close to the reflectometer. The quantitative agreement between the simulated and measured density profiles gives confidence that the edge plasma density in the presence of local gas puffing can be well predicted. The increase of plasma density in front of the antenna straps leads to an increase of ICRF coupling. Detailed calculations of the coupling resistance with different wave codes and the associated comparisons with experiments can be found in [10, 13].

These codes thus have developed a predictive capability to calculate and optimize the coupling also for future machines. Indeed, for these machines, while toroidaly uniform edge density profiles are usually available, the effect of the local gas puffing as well as the level of gas puffing needed to modify the local density profile to the extend needed for the coupling can now be ascertained.

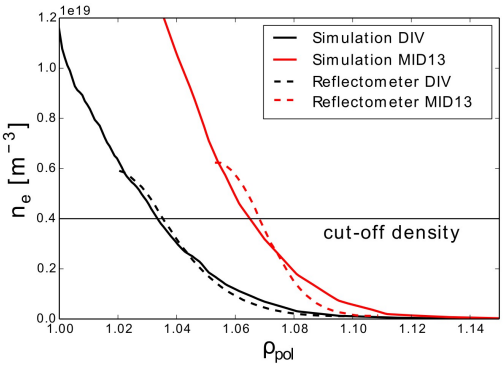

FIG. 4. Comparisons of the simulated and measured density profiles (L-mode) at the position of the reflectometer embedded in antenna #4 [14].

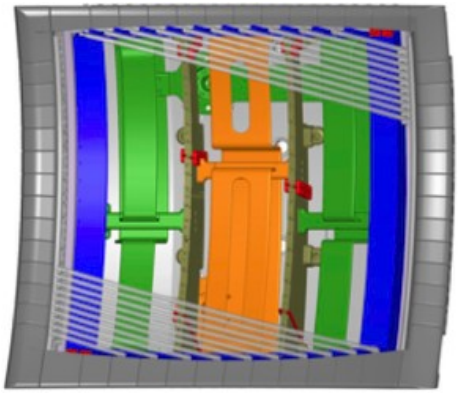

FIG. 5. New 3-strap antenna (Faraday screen partially removed). The width of the antenna is 1.06 m, the height 1.22 m.

3. Enhanced plasma-antenna interaction

Central ICRF heating was systematically used in the all-metal ASDEX Upgrade to counter the density and impurity peaking in high density plasmas as long as the antenna limiters were still made of carbon [15]. From 2006 on, when the antenna limiters were also coated with W, the use of ICRF was limited to high density/ high gas puffing scenarios, since otherwise the W release in the plasma would be too high W.

The hypothesis was that the increased W release is due to the acceleration of ions in sheaths and resulting sputtering, that those sheaths are a consequence of parallel (to B) RF electric fields $E_{//}$, which themselves are due to induced current driven at inappropriate locations. New 3-strap antennas [16, 17, 18] in ASDEX Upgrade were designed to cancel these undesirable induced currents: the currents induced in the antenna frame by the central strap (in orange in *FIG. 5)* can to first order be compensated by an appropriate choice (in amplitude and phase) of the currents in the outer straps (in green in *FIG. 5*). Theoretical calculations [19] with HFSS, including the plasma as an isotropic, absorbing medium, confirm that the RF electric fields $E_{//}$

near the limiters are substantially lower for the 3-strap antenna than for the 2-strap antenna (see *FIG. 6*).

3.1. Reduced impurity production

The decrease of the electric fields and corresponding reduction of the sheaths leads indeed to a strong reduction of impurity production. *FIG. 7* shows the increase in W impurity concentration in the plasma, during phases when the original W-coated 2-strap antennas are energized, as compared to phases when the B-coated 2-strap antennas are in operation.

In contrast to this, *FIG. 8* shows that the W concentration in the phase when the W-coated 3-strap antenna is energized is not higher than when the B-coated 2-strap antennas are in operation. Direct measurements of the impurity production at the limiters of the W-coated antennas [17] show a reduction by a factor of 2 between the 3-strap and the 2-strap antennas.

3.2. Effect of the ICRF power on the density profile in front of the antenna.

The rectified sheaths, a consequence of the RF electric fields, which result in an enhanced impurity production have a second effect: a change of the density profile in front of the antenna.

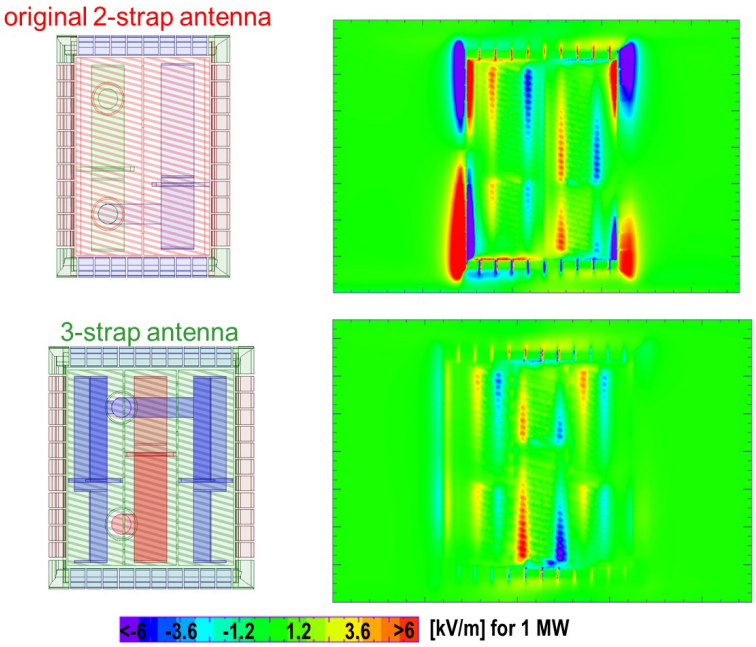

FIG. 6. Comparison of $E_{//}$ calculated with HFSS for the original 2-strap and the new 3-strap antenna for 1 MW launched. Note: asymmetries in the toroidal position of the feeders (clearly seen on the left pictures) are due to boundary conditions of AUG.

The rectified electric fields lead to different potentials on adjacent magnetic field lines and thus to radial DC electric fields (perpendicular to the field lines). These in turn, combined with the magnetic field, cause ExB convective patterns, which will change the density in front of the antenna. To understand and calculate (self-consistently) the change in density profiles in front of the antenna involves several interrelated phenomena: energy and particle transport inside the plasma, generation and propagation of EM fields and boundary conditions in semi-closed volumes.

These phenomena occur with different temporal and spatial scales. The problem is thus split in different parts and evaluated iteratively. The iterative procedure starts with the numerical code EMC3-Eirene [10], which allows the construction of a 3D density profile throughout the whole tokamak. The second step is to calculate the RF fields for the given density profile. These RF fields are obtained from the antenna code RAPLICASOL (Radiofrequency wAve couPLing for Ion Cyclotron Antenna in Scrape-Off-Layer) [20]. It is a 3D full-wave Finite Element code which calculates

the radiofrequency electromagnetic fields in the cold plasma approximation in the neighbourhood of a realistic antenna geometry for a given density profile (up to 3D). The third step is to model the formation of the sheaths, given the density profile and the corresponding RF fields. The parallel component of the electric field $E_{//}$, calculated by RAPLICASOL, is then passed to a self-consistent sheath and wave model SSWICH (Self-consistent Sheaths and Waves for Ion Cyclotron Heating) [21]. It is a three fluid model that calculates the slow wave propagation with the nonlinear sheath boundary conditions (SBC) on the antenna limiters, the RF sheaths excitation and the DC plasma biasing. The presently used version of SSWICH-SW makes the assumption that $E_{//}$ is only due to the slow wave. Unlike RAPLICASOL and EMC3-Eirene, SSWICH is essentially 2D. To get the sheath behaviour throughout the whole 3D antenna, the 2D SSWICH code is run several times on consecutive slices in independent simulations to emulate a pseudo-3D scheme by assuming that poloidal derivatives can be neglected. The slices are not purely horizontal, but in a radial-parallel plane. To satisfy the existence of a slow wave only, the magnetic field can either be parallel or perpendicular to walls. Nonlinear sheath boundary conditions on the antenna limiters are enforced on perpendicular walls to the background magnetic field. SSWICH currently supports three sheath models [21, 22, 23]. In *FIG. 9*, DC potentials calculated by SSWICH are shown for the 2-strap and 3-strap antenna assuming for simplicity a 1D density profile. The power balance for the 2-strap antenna is 1/2,1/2 (equal power on both ports) and for the 3-strap antenna it is 1/3 outer, 2/3 central. The 3-strap antenna clearly has a lower DC potential than the 2-strap antenna. The iterative loop is finally closed by passing the DC potential calculated by SSWICH back to EMC3-Eirene, which uses it to calculate the $E \times B$ drifts and a new density profile.

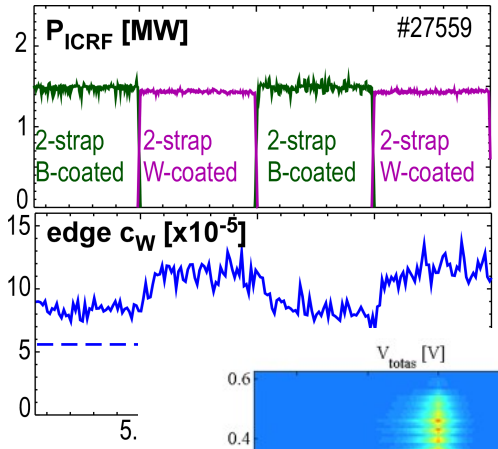

FIG. 7 Time when poweri 2-strap and t

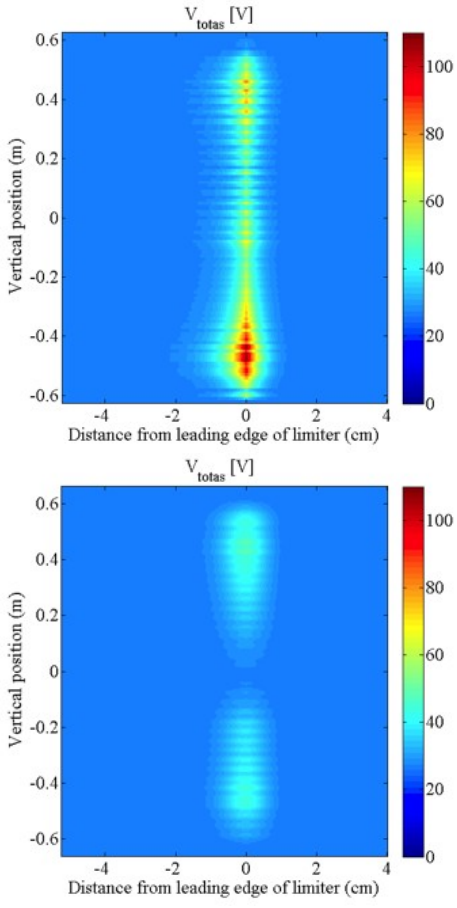

FIG. 9. Top: DC potential as a function of (x) radial distance from the leading edge of the limiter and (y) the vertical antenna dimension for 2-strap antenna. Bottom: DC potential for 3-strap antenna.

Density profiles calculated with this self-consistent simulation [24] can be compared to direct measurements of the local density profiles in front of the 3-strap antenna with the recently reflectometers installed in antenna #3. A "semi-simulation", where the experi-mentally measured DC potential (obtained from a reciprocating retarded field analyser) is used rather than the calculated value, as input for EMC3-Eirene to evaluate the ICRF induced $E \times B$ drifts and the resulting self-consistent density profiles has already been performed. These profiles are in good agreement with measurements [25].

With these methods, the mechanisms of density convection induced by ICRF can be

explained, the modified density in different conditions (different plasma scenarios, different antenna phasings) predicted and many related physics such as erosion and W sputtering on the antenna can be explored.

IShTAR [26], a dedicated test stand which offers a better control of the antenna environment, more access and operational time for dedicated diagnostics will allow to refine the set of theoretical tools by measuring directly the electric field in the plasma sheath, the driving parameter of the process.

4. Conclusions and Future Developments

The combination of experiments, new measurement capabilities and theory has led to a better understanding of the antenna coupling, density profiles in front of the antenna as well as of the origin of the sheaths, and thus to a solidly grounded approach to design antennas with good coupling and reduced impurity production.

A new 360° toroidally distributed antenna concept [5, 27, 28] proposed for DEMO takes advantage of this progress. It can be designed to be inherently matched and thus much less sensitive to edge density variations. Improved coupling will result from the combination of operation at low $k_{//}$ and gas puffing. With its 360° symmetry, it conceptually avoids the main undesired induced currents as occur in the frame of an antenna with limited toroidal extend and thus substantially reduces the occurrence of sheaths. The optimization of the DEMO antenna will benefit from the availability of the newly developed and benchmarked codes.

Acknowledgements

This work has been carried out within the framework of the EUROfusion Consortium and has received funding from the Euratom research and training programme 2014-2018 under grant agreement No 633 053. The views and opinions expressed do not necessarily reflect those of the European Commission.

References

[1] GOULDING, R., et al., RF Power in Plasmas (Palm Springs, 1995), AIP, NY (1996) **355**, 397-400.
[2] NOTERDAEME, J.-M., et al., Fusion Energy, (Montreal, 1996), IAEA, **3**, 335-342.
[3] NOTERDAEME, J.-M., Fusion Eng. Des. **74** (2005) 191-198.
[4] MONAKHOV, I., et al., Fusion Eng. Des. **74** (2005) 467-471.
[5] RAGONA, R. and MESSIAEN, A., Nucl. Fusion **56** (2016) 076009.
[6] STEPANOV, I., et al., Nucl. Fusion **55** (2015) 113003.
[7] LANCELLOTTI, V., et al., 2006 Nucl. Fusion **46** S476.
[8] FENG, Y., et al., Contributions to Plasma Physics **44** (2004) 57-69.
[9] REITER, D., et al., Fusion Science and Technology **47** (2005) 172-86.
[10] ZHANG, W., et al., Nucl. Fusion **56** (2016) 036007.
[11] AGUIAM, D.E., et al., Rev. Sci. Instrum., **87** (2016) 3–5.
[12] AGUIAM, D.E., et al., "X-mode raw data analysis of the new AUG ICRF antenna edge density profile reflectometer" SOFT2016, to be publ in Fusion Eng. Des.
[13] ZHANG, W., et al., "3D simulations of gas puff effects on edge plasma and ICRF coupling in JET", submitted to Nucl. Fusion.
[14] ZHANG, W., et al., "Investigation of ITER-like gas injection in AUG" to be subm. to Nucl. Fus.
[15] DUX, R., et al., J. Nucl. Mater **363–365** (2007) 112–116.
[16] BOBKOV, V., et al., "Making ICRF power compatible with a high-Z wall in ASDEX Upgrade", EPS2016, accepted for publication in Plasma Phys. Control. Fusion.
[17] BOBKOV, V., et al., Nucl. Fusion **56** (2016) 084001.
[18] FUENFGELDER, H., et al., "The international cooperation to build the new ICRF antennas on ASDEX Upgrade and the results obtained", SOFT2016, to be published in Fusion Eng. Des.
[19] BOBKOV, V., Nucl. Fusion **53** (2013) 093018.
[20] JACQUOT, J., et al., AIP Conf. Proc. **1689** (2015) 050009.
[21] COLAS, L., et al., 2012 Phys. Plasmas **19** (2012) 092505.
[22] LIEBERMANN, M., et al., IEEE Plasma Sci. **16** (1988) 638.
[23] BRINKMANN, J., et al., Phys. D: Appl. Phys. **42** (2009) 194009.
[24] ZHANG, W., et al., "Self-consistent simulations of edge plasma convection in the presence of RF waves", to be submitted to Nucl. Fusion.
[25] ZHANG, W., et al., Plasma Phys. Control. Fusion **58** (2016) 095005.
[26] CROMBE, K., et al., "IShTAR, a helicon plasma source to characterize the interaction between ICRF and Plasma", **EX/P6-48**, this conference.
[27] BOSIA, G., et al., Fusion Eng. Des. **92** (2015) 8-15.
[28] BADER, A., et al., "ICRF Power for DEMO", **FIP/P7-13**, this conference